

Families of Halo-like invariant tori around L_2 in the Earth-Moon Bicircular Problem*

José J. Rosales, Àngel Jorba, and Marc Jorba-Cuscó

Departament de Matemàtiques i Informàtica
Barcelona Graduate School of Mathematics (BGSMath)
Universitat de Barcelona (UB)
Gran Via de les Corts Catalanes 585, 08007 Barcelona, Spain
E-mails: rosales@maia.ub.es (✉), angel@maia.ub.es, marc@maia.ub.es

February 29, 2020

Abstract

The Bicircular Problem (BCP) is a periodic time dependent perturbation of the Earth-Moon Restricted Three-Body Problem that includes the direct gravitational effect of the Sun. In this paper we use the BCP to study the existence of Halo-like orbits around L_2 in the Earth-Moon system taking into account the perturbation of the Sun. By means of computing families of 2D invariant tori, we show that there are at least two different families of Halo-like quasi-periodic orbits around L_2 .

Keywords: Translunar point · Quasi-periodic Halo orbits · Stability of invariant curves

*This work has been supported by the Spanish grant PGC2018-100699-B-I00 (MCIU/AEI/FEDER, UE) and the Catalan grant 2017 SGR 1374. The project leading to this application has received funding from the European Union's Horizon 2020 research and innovation programme under the Marie Skłodowska-Curie grant agreement #734557.

| | | |
|----------|--|-----------|
| 1 | Introduction | 3 |
| 2 | From RTBP to BCP: the L_2 point case | 5 |
| 3 | Approach to study the vicinity of L_2 | 8 |
| 3.1 | Computation of highly unstable invariant tori | 9 |
| 3.2 | Linear stability | 11 |
| 3.3 | Initial condition and continuation of invariant tori | 13 |
| 4 | Dynamics around the L_2 point | 14 |
| 4.1 | The Type I and Type II Halo-like families | 15 |
| 4.1.1 | Stability | 22 |
| 4.2 | Applications | 22 |
| 5 | Conclusions and further work | 25 |
| 6 | Appendix | 26 |
| | References | 29 |

1 Introduction

In recent years, major space agencies have shown interest in concepts that involve using the Moon and its neighboring area as candidates to host space assets to support scientific missions or commercial endeavors. An example is the Lunar Gateway, a permanent space station planned to orbit around the Moon. Other classical examples are the study of the far side of the Moon and the aim to exploit the cislunar space by using the invariant structures related to L_1 .

The basic model to study the dynamics of a spacecraft in the Earth-Moon system is the Restricted Three Body Problem (RTBP) with the Earth and the Moon as primaries. The most usual formulation of the RTBP is the circular version. In this model, it is assumed that the Earth (E) and the Moon (M) revolve along a circular orbit centered in their common barycentre (B). It is standard to consider a synodic reference frame, that is, a rotating frame that fixes the primaries at the horizontal axis. This model, although an excellent starting point, fails to capture some relevant features of the real Earth-Moon system. For example, the direct effect of the gravitational field of the Sun (S), or the eccentricity of the Moon's orbit. Focusing our attention on the Sun's gravity as a major perturbation force, the natural question is to look for models that account for this effect. One model that considers the combined effect of the Sun, Earth, and Moon on an infinitesimal particle is the Bicircular Problem (BCP), see Huang [1960], Cronin et al. [1964].

In the BCP, the dynamics of the Earth, Moon and Sun are simplified considering that the three bodies orbit in the same plane. Also, it is considered that the Earth and the Moon follow a circular orbit around their barycenter (as in the RTBP), and that B is orbiting around the S-E/M barycenter. Note that this model is not coherent, in the sense that the motion of the three massive bodies is not described by the Newton's equations of motion.

Using the frame and the units of the RTBP, with the origin in the Earth-Moon barycenter, the x -axis rotating such that the Earth and the Moon are sitting on it, and considering the momenta $p_x = \dot{x} - y, p_y = \dot{y} + x, p_z = \dot{z}$, the BCP admits a Hamiltonian formulation as follows:

$$H_{BCP} = \frac{1}{2}(p_x^2 + p_y^2 + p_z^2) + yp_x - xp_y - \frac{1-\mu}{r_{PE}} - \frac{\mu}{r_{PM}} - \frac{m_S}{r_{PS}} - \frac{m_S}{a_S^2}(y \sin \vartheta - x \cos \vartheta) \quad (1)$$

where $r_{PE}^2 = (x-\mu)^2 + y^2 + z^2$, $r_{PM}^2 = (x-\mu+1)^2 + y^2 + z^2$, $r_{PS}^2 = (x-x_S)^2 + (y-y_S)^2 + z^2$, $x_S = a_S \cos \vartheta$, $y_S = -a_S \sin \vartheta$, and $\vartheta = \omega_S t$ with ω_S being the frequency of the Sun around the Earth-Moon barycenter. The parameters of the BCP used here are captured in Table 1. Note that in this reference system the Sun moves around the origin in a circular motion (See Figure 1). For the details on the derivation of the BCP equations of motion, the interested reader is referred to Gómez et al. [2001a]. An important observation is that

Table 1: Parameters of the BCP.

| | |
|---------------------------------|---------------------------------|
| $\mu = 0.0121505816234336$ | $m_s = 328900.5499999991152436$ |
| $\omega_s = 0.9251959855182896$ | $a_s = 388.8111430233511214$ |

the Hamiltonian (1) depends periodically on time. This periodic effect captures the direct gravitational influence of the Sun. Moreover, Hamiltonian (1) can be expressed as a time-periodic perturbation of the RTBP,

$$H_{BCP}(X, P_X, \vartheta) = H_{RTBP}(X, P_X, \vartheta) + H_S(X, P_X, \vartheta),$$

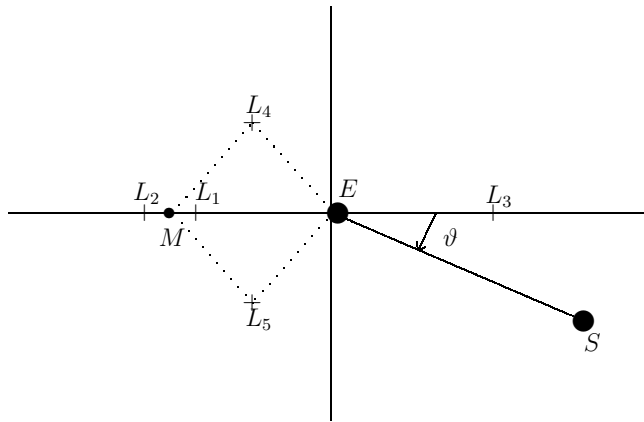


Figure 1: Sketch of the Bicircular problem. The points $L_{1,\dots,5}$ are the Lagrangian (equilibrium) points of the Earth-Moon RTBP.

where $X = (x, y, z)$, $P_X = (p_x, p_y, p_z)$, H_{RTBP} is the Hamiltonian of the RTBP, and H_S is the Hamiltonian associated to the perturbation due to the Sun. The consequences on the dynamics of this periodic time-dependency will be explained later.

The BCP has been used in previous works to explore the dynamics around the Earth-Moon libration points. The L_1 point is explored in Jorba et al. [2020]. The main takeaway is that in the BCP, similarly to the RTBP, the planar Lyapunov family undergoes a (quasi-periodic) pitchfork bifurcation giving rise to two families of quasi-periodic Halo orbits. The neighborhood of L_3 is studied in Jorba and Nicolás [2020] and the dynamics around the L_4 and L_5 triangular points has been analyzed in Simó et al. [1995], and Castellà and Jorba [2000], where families of 2D tori in an extended neighborhood of the triangular points were computed. This paper focuses on the dynamics around the L_2 point in the BCP and, to the best knowledge of the authors, it has not been studied yet.

It is worth noting that there are other models describing the dynamics of a particle in the Earth-Moon system that account for the effect of the Sun. For example, the Quasi-Bicircular (QBCP) problem. As opposed to the BCP, the QBCP is coherent and the motion of the three primaries is a solution of a three-body problem. The QBCP can also be formulated as a time-periodic perturbation of the RTBP. Hence, from a formulation point of view, the motion of the primaries is the only difference between the two models. (See Andreu [1998] for the details on the QBCP derivation). Another relevant model that describes the motion of a test particle in the Sun-Earth-Moon is the Hill restricted four body problem, introduced by Scheeres [1998].

Focusing on the BCP and QBCP, it is interesting to mention that despite modeling the same system, there are qualitative differences between these two models around L_2 . (See Jorba-Cuscó et al. [2018] for a discussion.) Thus, it is important to address the question of why we chose the BCP over the QBCP to study the dynamics around L_2 . There are two main motivations: the first one is that the BCP, although being the simplest model that captures the dynamics of the Sun-Earth-Moon system, is not fully understood around L_2 . Hence, from a strictly academic point of view, and for the sake of completeness, it is interesting to understand the dynamics around L_2 .

The second motivator has in mind mission analysis. As mentioned, both the BCP and the QBCP attempt to model the same system, but they behave differently around

L_2 . Understanding the transition between the RTBP and the BCP and QBCP could shed some light on how sensitive the Earth-Moon system is to perturbations, and pave the way to approaches that could ease the transition from simplified models around L_2 to the full ephemeris model. This paper does not attempt to answer these questions, but is a step in that direction. Finally, mention that all the tools and techniques described in this paper are model-agnostic, and could be applied to the QBCP or other models that depend periodically on time.

As we have mentioned, in this paper we explore the neighborhood of the translunar point in the BCP. In particular we are interested in the counterparts (in the BCP) of the well-known Halo families (see Breakwell and Brown [1979]). In this model, the Halo families are no longer composed by periodic orbits but by quasi-periodic orbits with two basic frequencies, one coming from the Halo orbits of the RTBP plus the frequency ω_S . To compute these families we use a combination of a method to approximate invariant curves with multiple shooting, with the continuation method to generate a complete atlas of the dynamical equivalents of the Lyapunov and Halo families near the translunar point. Notice that, due the absence of a natural replacement of L_2 , the properties of some of these families change near the translunar point (now only geometrically defined in the BCP). In particular, we report the existence of a family of Halo-like orbits that does not come from the original Halo family in the RTBP.

This paper is structured as follows: Section 2 contains an analysis of the effect that the Sun, as modeled in the BCP, has on the L_2 point. This serves as a motivation for Section 3, where after a brief discussion on two approaches to study the dynamics around the L_2 point, the method of tori continuation is justified as appropriate for the L_2 region and explained. Section 3 also includes the strategy employed to find the different families. Section 4 elaborates on the results obtained from tori continuation, focusing on the Halo-like tori and their stability. The focus in Halo-like orbits is not arbitrary, and it responds to the application these trajectories have for lunar missions. This is also discussed in Section 4. Finally, Section 5 presents the conclusions and further work.

2 From RTBP to BCP: the L_2 point case

It is well known that L_2 is an equilibrium point of the RTBP. However, as opposed to the RTBP, the BCP is not an autonomous system, and it depends periodically on time so that the L_2 point is not an equilibrium point anymore. In a general setting (not necessarily Hamiltonian), if a periodic perturbation is applied to a differential equation then, under generic conditions of non-degeneracy, an equilibrium point becomes a periodic orbit with the same period as the perturbation. Applying this principle, in this section we explain what are the dynamical consequences that the time-periodic perturbation has on the L_2 point in the context of the BCP.

The approach taken to study the transition of the L_2 point from the RTBP to the BCP is by continuation with respect to the mass of the Sun. To that effect, we define the following family of Hamiltonians,

$$H^\varepsilon = H_{RTBP} + \varepsilon H_S, \quad (2)$$

with $\varepsilon \in [0, 1]$. Note that for $\varepsilon = 0$, $H^0 = H_{RTBP}$, and for $\varepsilon = 1$, $H^1 = H_{BCP}$. Considering $\varepsilon = 0$, the five Lagrange points ($L_i, i = 1, \dots, 5$) are equilibrium points of the system (2). When $|\varepsilon|$ is small enough, the equilibrium points become periodic orbits around the point L_i (now defined only geometrically since they are no longer equilibrium points) with the

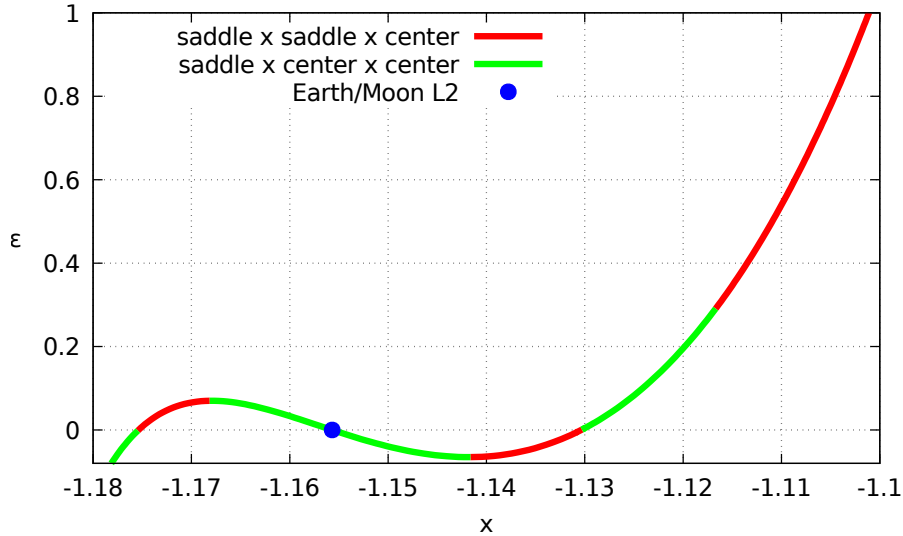


Figure 2: Stability type of the periodic orbits as a function of ε starting at E/M L_2

same period as the perturbation. In our case, the period is equal to the period of the Sun, $T = 2\pi/\omega_S$. However, the perturbation that defines the BCP cannot be considered small. For example, around the triangular points L_4 and L_5 there is a loss of uniqueness of the periodic orbit, and three periodic orbits appear (see Gómez et al. [2001b], Simó et al. [1995]). The size of the perturbation also affects the L_2 point.

Besides showing the existence of these periodic orbits, computing their stability is essential to have the full picture. By means of analyzing the spectra of the monodromy matrix, we also show how the linear stability of these new periodic orbits evolves with respect to the continuation parameter ε . It is important to note that due to the highly unstable nature of the L_2 region, the algorithm to compute periodic orbits had to be implemented using a multiple shooting scheme. This is a pretty standard procedure (see Stoer and Bulirsch [2002], Seydel [2009]) and the details can be found in Gómez and Mondelo [2001] for the RTBP. For the present work, the total number of sections used was four.

The results of continuing the L_2 point with respect to the mass of the Sun are shown in Figure 2. The horizontal axis is the x component of the periodic orbit at $\theta = 0$, and the vertical axis is the continuation parameter ε applied to the mass of the Sun. Starting from L_2 , and moving to the left the parameter increases until it hits a local maximum, and then decreases to cross the horizontal line and become negative. The point on the horizontal axis corresponds to a 1:2 resonant planar Lyapunov orbit (the frequency of the orbit is twice the frequency of the Sun). Moving from L_2 to the right, the continuation parameter becomes negative, decreasing until it hits a local minimum, and then increases to cross the horizontal line and reach the BCP ($\varepsilon = 1$). Again, in this case the continuation also crosses the horizontal axis. This corresponds to the same 1:2 resonant planar Lyapunov orbit. The main takeaway is that there is no natural dynamical substitute of the L_2 point in the BCP because there is no direct connection between it and a periodic orbit in the BCP. The periodic orbit around L_2 in the BCP is pictured in Figure 3. The L_2 point and the Moon are added for reference.

Figure 2 also contains the details on the linear stability of the periodic orbits computed. As a technical remark, for the computation of the eigenvalues of the monodromy matrix,

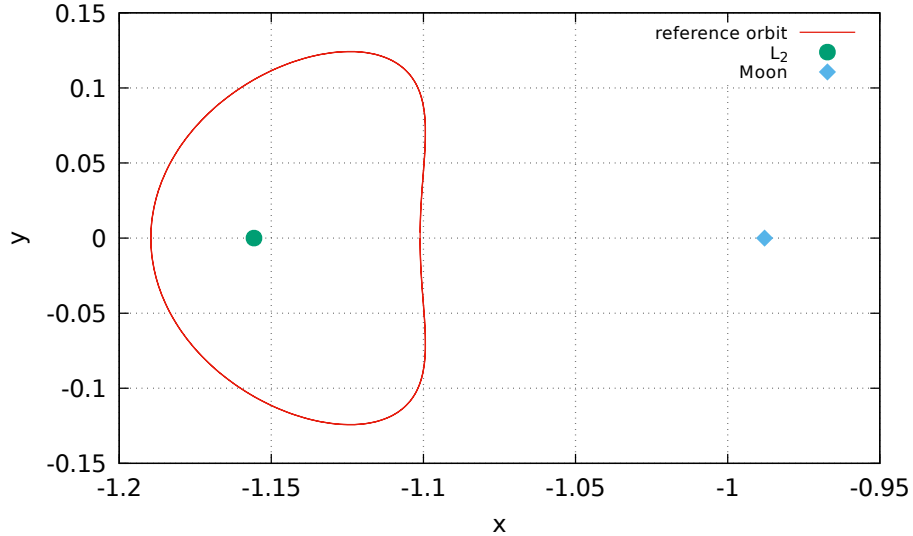


Figure 3: Periodic orbit near L_2 in the BCP. (Note: In the figure is not perceived, but the periodic orbit revolves around the L_2 twice in one period.)

the approach described in Gonzalez and Mireles James [2016] was used to account for the fact that multiple section were used. It is observed that the periodic orbits alternate between the types saddle \times center \times center (green regions) and saddle \times saddle \times center (red regions). Starting from L_2 , the linear stability is of the type saddle \times center \times center. Moving to the left, ε increases and the periodic orbits keep this linear stability type until they hit the local maximum. In this turning point, the linear stability becomes of the type saddle \times saddle \times center until another bifurcation point at resonant 1:2 planar Lyapunov ($\varepsilon = 0$). At this point, ε becomes negative, and the resulting periodic orbits are of the type saddle \times center \times center. A similar pattern but with different sign for ε is observed when moving to the right of the L_2 point. In this scenario, ε decreases and maintains the same linear stability type as L_2 until they hit a local minimum. As before, in this turning point, the linear stability becomes of the type saddle \times saddle \times center until $\varepsilon = 0$, where there is yet another bifurcation. At this bifurcation, the linear stability becomes of the type saddle \times center \times center. Finally, this resonant planar Lyapunov orbit is continued until the last bifurcation point. This is a pitchfork bifurcation, and it is where the 1:2 resonant (with the Sun) Halo orbit in the RTBP ends (see Andreu [1998] for the details). The implication is that the 1:2 resonant Halo orbit in the RTBP does not reach the BCP. As we will see in Section 4, this is not the case for all Halo orbits, and there is a dense set of Halo orbits that survive the perturbation of the Sun as modeled in the BCP.

After this point, the stability of the periodic orbits is of the type saddle \times saddle \times center until $\varepsilon = 1$. The eigenvalues $\lambda_i, i = 1, \dots, 6$ of the monodromy matrix associated to the periodic orbit in the BCP are captured in Table 2.

As final remark, it is important to note that the nature of the perturbation shapes the dynamics around an equilibrium point. The comparison between the BCP and QBCP illustrates this phenomena. In the QBCP the L_2 is replaced by a periodic orbit that is small in the sense that its maximal distance to L_2 is of the order of 10^{-6} , and it has the same stability type of the L_2 point. See Andreu [2002], Jorba-Cuscó et al. [2018] and references therein for the details.

Table 2: Eigenvalues of the monodromy matrix related to the periodic orbit displayed in Figure 3. Due to the Hamiltonian nature of the system, the other three eigenvalues are $\lambda_i^{-1}, i = 1, 2, 3$. Also, note that due to the non-autonomous character of the BCP Hamiltonian, there is no double eigenvalue 1.

| | $\text{Re}(\lambda_i)$ | $\text{Im}(\lambda_i)$ |
|-------------|-------------------------|------------------------|
| λ_1 | 776607.1046490771695971 | 0.0000000000000000 |
| λ_2 | 1.6602116402354583 | 0.0000000000000000 |
| λ_3 | 0.8656940044785918 | -0.5005735616368709 |

3 Approach to study the vicinity of L_2

To study the dynamics of a dynamical system, a typical approach is to look for invariant objects and analyze their stability. Typically, the analysis starts looking for equilibrium points, then periodic orbits, 2D tori, and so on. Section 2 covered the analysis of the periodic orbit with the same period as the effect of the Sun. However, this does not provide the full picture and gives little insight on the dynamics around the L_2 point.

One approach to get the full picture of the dynamics is to do a reduction to the center manifold of the periodic orbit. This approach consists in a series of changes of variable to decouple the saddles from the centers. This decoupling allows to reduce the dimension of the system, and to focus only on the invariant objects that live in the center manifold. This technique has been proven very successful to characterize the dynamics around the collinear points in the RTBP (Jorba and Masdemont [1999]) for different mass parameters; around the L_1 point the BCP (Jorba et al. [2020]) and L_2 in the QBCP (Andreu [2002], Le Bihan et al. [2017]); or around the L_1 and L_2 points in the Sun-Earth RTBP for solar sails Farrés and Jorba [2010]. Note that the systems that can be studied with this technique are very broad: the reference (Jorba and Masdemont [1999]) deals with autonomous Hamiltonians, the references (Jorba et al. [2020]), Andreu [2002], and Le Bihan et al. [2017] with Hamiltonians that depend periodically on the time, and the reference Farrés and Jorba [2010] with general Ordinary Differential Equations. The interested reader is referred to Carr [1981], Sijbrand [1985], Vanderbauwhede [1989] for a more general treatise on the center manifold and its applications. The main advantage of this method is that it provides a comprehensive picture of orbits staying in a neighborhood of an invariant object and its bifurcations. The disadvantages are that, due to the construction of the center manifold, the neighborhood where it is valid may be very small due to the presence of small divisors.

An alternative to the center manifold is to directly compute the families of invariant objects that shape the phase space of the dynamical system (equilibrium points, periodic orbits, 2D tori and so on). A key advantage of this approach is that it can be applied far away from L_2 . Also, in some cases (equilibrium points, periodic orbits, and 2D tori) there are techniques to compute the stability of each member of the family. The main limitation of this approach is that computing tori of dimension higher than 2 is very expensive computationally (Jorba and Olmedo [2009]) and, sometimes, cumbersome. In the context of the BCP, in Castellà [2003] computed families of 3D tori around the triangular points.

In addition to that, the continuation of these objects involves some level of trial and error, and once the continuation process starts, a lot of fine tuning due to the presence of resonances is needed. Finally, and as opposed to the center manifold approach, this method provides an incomplete picture unless all relevant invariant objects are computed.

Note that the latter approach assumes the existence of families of invariant objects. The

assumption deserves some explanation. In the context of the BCP, the existence of invariant tori is inherited from the RTBP. It is well known that around the collinear equilibrium points of the RTBP there are families of periodic orbits (planar and vertical Lyapunov, and Halo orbits) and quasi-periodic orbits (quasi-halos and Lissajous). See Jorba and Masdemont [1999] and Gómez and Mondelo [2001] for details. Under generic conditions of non-resonance and non-degeneracy, adding a small enough periodic (or quasi-periodic) time-dependent perturbation to RTBP, causes the existing invariant objects to inherit the frequencies of the perturbation. It is important to mention that the families of invariant objects become Cantorian because only those frequencies satisfying a suitable non-resonance condition survive. As a consequence, the families of objects are Cantorian, not continuous. The details on the proofs that back these statements can be found in Jorba and Villanueva [1997]. Finally, an example of this phenomena in the context of the RTBP and the BCP can be found in Jorba et al. [2020].

The study of the L_2 region in the BCP was initially approached using the reduction to the center manifold. Actually, the code used to generate the results in Jorba et al. [2020] for L_1 in the BCP, was initially developed to study the neighborhood of L_2 . However, the radius of convergence of the computed center manifold was very small, and it was concluded that this approach was not suitable for L_2 . Hence, it was decided to compute families of 2D tori around the L_2 region along with their stability following the methods described Castellà and Jorba [2000] and Jorba [2001], respectively. The next subsections outline the numerical methods to compute invariant tori, their stability, and the continuation strategy.

3.1 Computation of highly unstable invariant tori

The method used to compute invariant tori is based on Castellà and Jorba [2000]. The general statement of the problem is the following: assume there exists a quasi-periodic orbit $x(t)$ with two basic frequencies $\omega_1, \omega_2 \in \mathbb{R}$ such that $\omega_1/\omega_2 \in \mathbb{R} \setminus \mathbb{Q}$. This means that there exists a map $X : \mathbb{T}^2 \rightarrow \mathbb{R}^6$ (the parametrization of the torus) such that $x(t) = X(\omega_1 t, \omega_2 t)$.

In the scenario of the BCP, one of the frequencies is equal to the frequency of the Sun (ω_S) so, from now on, $\omega_2 = \omega_S$. Now, let us define the stroboscopic map F as the flow of the BCP ϕ_{BCP} at time $T = 2\pi/\omega_S$. Note that now the closed curve $\theta \in \mathbb{T} \mapsto X(\theta, 0) \in \mathbb{R}^6$ is invariant by F ,

$$F(X(\theta, 0)) = X(\theta + \omega_1 T, \omega_S T) = X(\theta + 2\pi \frac{\omega_1}{\omega_S}, 2\pi) = X(\theta + 2\pi \frac{\omega_1}{\omega_S}, 0).$$

Setting $\rho = 2\pi \frac{\omega_1}{\omega_S}$ and denoting $X(\theta, 0) \equiv X(\theta)$ the previous invariance equation reads,

$$X(\theta + \rho) = F(X(\theta)). \tag{3}$$

Thus, knowing that one of the fundamental frequencies of the motion is ω_S , the problem of computing a torus is reduced to finding a function $\hat{X} : \mathbb{T}^1 \rightarrow \mathbb{R}^n$ that satisfies Equation (3) for a given ρ (note that to know ρ is equivalent to know ω_1). Such function \hat{X} is called an *invariant curve* with *rotation number* ρ . Obviously, if \hat{X} is an invariant curve with rotation number ρ , it satisfies that

$$G(\hat{X}(\theta)) = F(\hat{X}(\theta)) - \hat{X}(\theta + \rho) \equiv 0. \tag{4}$$

From a practical point of view, the approach is to find a zero of G . A convenient way to

approximate an invariant curve is to use its (truncated) Fourier series,

$$X(\theta) = a_0 + \sum_{k=1}^N a_k \cos(k\theta) + b_k \sin(k\theta) \quad a_i, b_i \in \mathbb{R}^n. \quad (5)$$

Hence, the goal is to compute the Fourier coefficients $a_i, b_i, i = 0, \dots, N$ such that they define a periodic function X which is a zero of (4). This leads to $(2N + 1)n$ unknowns. Hence, at least the same number of equations is required to solve for all $a_i, b_i, i = 0, \dots, N$. To this end, (4) is discretized by using an equispaced grid of values of θ such that

$$\theta_j = \frac{2\pi j}{2N + 1}, \quad j = 0, \dots, 2N \quad (6)$$

This provides the number of equations needed to solve for the Fourier coefficients $a_i, b_i, i = 0, \dots, N$. Finally, an extra equation specifying a value for the Fourier coefficients at $\theta = 0$ is required to resolve the ambiguity in the Fourier coefficients due to the fact that the map F is autonomous (see Castellà and Jorba [2000] for further details). This system of equations is solved by means of a standard Newton's method using least squares to account for the fact that we have more equations than unknowns.

In the same fashion as for the continuation of periodic orbits described in Section 2, the use of multiple shooting is required to mitigate the error growth due to the instability of the L_2 region (see Duarte [2020] for a discussion for the Sun-Jupiter $L_{1,2}$). We recall from Table 2 that the largest eigenvalue of the monodromy matrix of the periodic orbit around L_2 found in the BCP is of order of 10^6 . The following paragraphs illustrate how this is approached. Let us start with the following definition.

Definition 1. *Let g_1, \dots, g_r diffeomorphisms of some subset of \mathbb{R}^n into itself, let x be the parametric representation of a closed curve of \mathbb{R}^n , $\theta \in \mathbb{T}$ and let $\rho \in \mathbb{T}$. Then, x is called an ***r*-invariant curve** for g_1, \dots, g_r with rotation number ρ if*

$$(g_r \circ \dots \circ g_1)(x(\theta)) = x(\theta + \rho) \quad \forall \theta \in \mathbb{T}$$

Remark 1. *It is easy to check that if x is an *r*-invariant curve then, for any $\alpha \in \mathbb{R}$, $x(\theta + \alpha)$ is also a *r*-invariant curve. This implies that there are different sets of Fourier coefficients representing the same *r*-invariant curve.*

Given a *r*-invariant curve x_0 approximated by a truncated Fourier series (5), the goal is to compute its $(2N + 1)n$ coefficients $a_i, b_i, i = 0, \dots, N$. The invariance condition for a *r*-invariant curve reads

$$\begin{aligned} x_1(\theta) &= g_1(x_0(\theta)), \\ &\vdots \\ x_{r-1}(\theta) &= g_{r-1}(x_{r-2}(\theta)), \\ x_0(\theta + \rho) &= g_r(x_{r-1}(\theta)). \end{aligned} \quad (7)$$

As a result, to find x_0 , it is also required to solve for $x_i, i = 1, \dots, r - 1$. This is, there are a total of $(2N + 1)nr$ unknowns corresponding to all the *r*-invariant curves. Now, we use the grid (6) to discretized each of the equations in (7), and the following set of equations is

obtained,

$$G_r(x_0(\theta), \dots, x_{r-1}(\theta)) = \begin{bmatrix} g_1(x_0(\theta_0)) - x_1(\theta_0) \\ \dots \\ g_1(x_0(\theta_{2N})) - x_1(\theta_{2N}) \\ \vdots \\ g_r(x_{r-1}(\theta_0)) - x_0(\theta_0 + \rho) \\ \dots \\ g_r(x_{r-1}(\theta_{2N})) - x_0(\theta_{2N} + \rho) \end{bmatrix} = 0. \quad (8)$$

An extra equation specifying, for instance, a value of a coordinate at $\theta = 0$ is required to resolve the ambiguity in the Fourier coefficients (see Remark 1). The system of equations (8) is solved by means of a standard iterative Newton's method using least squares to account for the extra equation. The iteration process is stopped when the norm of the function becomes smaller than a prescribed tolerance (typically, a value of the order of 10^{-6} is good enough for plots, but for the computation of the stability we have used 10^{-10}). Note that this method ends up computing r curves.

This parallel shooting approach is useful to compute invariant curves for very unstable systems. In the case of interest, the L_2 region in the BCP, the maps g_j , $j = 1, \dots, r$ are defined as follows: if p denotes a point in the phase space, then

$$g_j(p) = \phi \left(p; (j-1)\frac{T}{r}, j\frac{T}{r} \right), \quad j = 1, \dots, r,$$

where $\phi(p; t_1, t_2)$ denotes the flow from time t_1 to time t_2 , and we recall that T is the period of the Sun. In this work, we use $r = 4$.

Note that the convergence of the Newton's method does not guarantee that the solution is a good representation of the torus. Remember that we have computed the torus based upon a truncated Fourier series (5). To estimate the error of the actual representation, the invariance condition is checked on a finer mesh. If the error in the verification of this condition is larger than a prescribed threshold, then more Fourier coefficients are added in the representation (5), and the process starts again.

3.2 Linear stability

To compute the stability of an invariant object is as important as the invariant object itself. The methods in this section are based on the results in Jorba [2001], that here we have adapted to a multiple shooting scheme. The following paragraphs provide an overview of the method to compute the stability of invariant curves, and the modification to work with unstable systems.

Let us assume that x is an invariant curve satisfying condition (3). To study the dynamical behavior close to the curve, we consider a small displacement $h \in \mathbb{R}^n$ with respect to x . Then,

$$F(x(\theta) + h) = F(x(\theta)) + D_x F(x(\theta))h + \mathcal{O}(\|h\|^2)$$

Hence, using that $F(x(\theta)) = x(\theta + \rho)$ and discarding the second order term, we have that the following dynamical system describes the linear normal behavior around the invariant curve,

$$\begin{aligned} \bar{h} &= A(\theta)h, \\ \bar{\theta} &= \theta + \rho, \end{aligned} \quad (9)$$

where $A(\theta) = D_x F(x(\theta))$ and $h \in \mathbb{R}^n$. Let $C(\mathbb{T}^1, \mathbb{C}^n)$ be the set of continuous functions between \mathbb{T}^1 and \mathbb{C}^n . If $\psi \in C(\mathbb{T}^1, \mathbb{R}^n)$, we define the operator $T_\rho : C(\mathbb{T}^1, \mathbb{C}^n) \rightarrow C(\mathbb{T}^1, \mathbb{C}^n)$ as $T_\rho(\psi(\theta)) = \psi(\theta + \rho)$, $\theta \in [0, 2\pi)$. In Jorba [2001] it is shown that:

- The stability analysis of an invariant curve of (3) is reduced to the following generalized eigenvalue problem,

$$A(\theta)\psi(\theta) = \lambda T_\rho(\psi(\theta)), \quad \lambda \in \mathbb{C}. \quad (10)$$

- If the Poincaré map is autonomous, then 1 is an eigenvalue of (10) with eigenfunction x' , where x denotes the invariant curve and $'$ the differentiation with respect to θ .
- Eigenvalues with norm 1 correspond to elliptic directions, and eigenvalues with norm different from 1 correspond to hyperbolic directions.

From a practical point of view, the goal is to solve a discrete version of (10). Details about how to deal with this problem numerically can be found in Jorba [2001], and will not be repeated here. In the following paragraphs we focus on how to adapt these methods to a multiple shooting scheme.

Let us assume that we have computed a r -invariant curve using a multiple shooting scheme with r sections, and that we want to know its stability. Using the same argument as before to construct the linearized dynamical system (9) and the generalized eigenvalue problem (10), the stability of the r -invariant curves is reduced to the analysis of the following generalized eigenvalue problem:

$$\underbrace{\begin{bmatrix} Dg_1 & 0 & \cdots & 0 & 0 \\ 0 & Dg_2 & \cdots & 0 & 0 \\ \vdots & \vdots & \ddots & \vdots & \vdots \\ 0 & 0 & \cdots & Dg_{r-1} & 0 \\ 0 & 0 & \cdots & 0 & Dg_r \end{bmatrix}}_{\mathcal{A}} \underbrace{\begin{bmatrix} \psi_1(\theta) \\ \psi_2(\theta) \\ \vdots \\ \psi_{r-1}(\theta) \\ \psi_r(\theta) \end{bmatrix}}_{\Psi(\theta)} = \lambda \underbrace{\begin{bmatrix} 0 & I & 0 & \cdots & 0 & 0 \\ 0 & 0 & I & \cdots & 0 & 0 \\ \vdots & \vdots & & \ddots & \vdots & \\ 0 & 0 & 0 & \cdots & 0 & I \\ T_\rho & 0 & 0 & \cdots & 0 & 0 \end{bmatrix}}_{\mathcal{B}} \underbrace{\begin{bmatrix} \psi_1(\theta) \\ \psi_2(\theta) \\ \vdots \\ \psi_{r-1}(\theta) \\ \psi_r(\theta) \end{bmatrix}}_{\Psi(\theta)}$$

where $g_k = g(x_k(\theta))$, $k = 1, \dots, r$, Dg_k is the differential evaluated on $x(\theta)$ and T_ρ denotes the operator $T_\rho : \psi(\theta) \mapsto \psi(\theta + \rho)$. In a more compact way, this eigenvalue problem can be expressed as

$$\mathcal{A}\Psi(\theta) = \lambda \mathcal{B}\Psi(\theta). \quad (11)$$

This generalized eigenvalue problem is solved identically as the case $r = 1$. The comments in Jorba [2001] apply also this formulation of the problem.

Note that in a simple shooting technique we compute the invariant curve for the map $g_r \circ \cdots \circ g_1$. In the same way, the stability for a single shooting invariant curve is given by the eigenvalue problem

$$(Dg_r \circ \cdots \circ Dg_1)\psi(\theta) = \lambda\psi(\theta + \rho). \quad (12)$$

The relation between the eigenvalues obtained when using single shooting with the ones obtained with parallel shooting is given by the next proposition.

Proposition 1. *If λ and $\Psi = (\psi_1, \dots, \psi_r)$ are an eigenvalue and its associated eigenfunction of (11), then λ^r and ψ_1 are an eigenvalue and its associated eigenfunction of (12).*

Proof.

$$\begin{aligned} (Dg_r \circ \dots \circ Dg_1)(\psi_1(\theta)) &= (Dg_r \circ \dots \circ Dg_2)(\lambda_1 \psi_2(\theta)) = (Dg_r \circ \dots \circ Dg_3)(\lambda_1^2 \psi_3(\theta)) \\ &= \dots = Dg_r(\lambda_1^{r-1} \psi_{r-1}(\theta)) = \lambda_1^r T_\rho(\psi_1(\theta)) = \lambda_1^r \psi_1(\theta + \rho). \end{aligned}$$

□

3.3 Initial condition and continuation of invariant tori

As mentioned at the beginning of this section, obtaining a first invariant curve is one of the main challenges. We will use as starting point for a family of invariant tori a periodic orbit which in the Poincaré map is a fixed point of centre×saddle type. Hence, we can use as first approximation the linearization of the Poincaré section around this fixed point. The initial frequency of this invariant curve is set to be $\rho = \omega_L + \Delta\rho$, where ω_L is the frequency of one the elliptic directions of the periodic orbit and $\Delta\rho$ is a small increment. The sign of $\Delta\rho$ is positive or negative depending on whether the frequency increases or decreases when moving away from the periodic orbit along the selected elliptic direction. Then, with this initial approximation, the Newton method is applied as described in Section 3.1.

Hence, for now on, let us assume that a torus as expressed in (5) is known. The strategy employed here to continue a family of tori is to parametrize the family with respect to the rotation number. To find a new torus of the family the rotation number is slightly increased (or decreased, depending on which direction the family wants to be continued) as it was done to find the first torus, and then the Newton method is applied to solve for the new torus as described in Section 3.1. In this sense, by modifying the rotation number we are using the current torus a seed for the Newton process. This is done until three tori are computed. After the third torus, the initial condition for the next tori of the family and the rotation number are obtained by interpolating the coefficients and the rotation numbers of the previous three tori, and extrapolating them to the new one by an increment ds . This provides a good enough initial guess to find the torus in a few iterations of the Newton method.

This particular implementation of the method does not consider the rotation number as a variable, and as such it is not estimated during the Newton process. This was implemented, and no significant benefit was identified. In order to keep the number of iterations low, the extrapolation step ds needs to be adjustable. The strategy followed is to double the extrapolation step if the number of iterations is less than 6, and divide it by two if it is greater.

The process of continuing tori is not absent of challenges. Hence, we consider relevant to address the main issue found during the continuation: the sensitivity to resonances. As mentioned at the beginning of this section, the family is Cantorian. This means that it has empty interior and positive Lebesgue measure (Jorba and Villanueva [1997]). The gaps in this family are due to resonances and, typically, they are small. Hence, the continuation process jumps over them. However, there are some instances where these gaps are too big and the continuation process has difficulties to continue. In this scenario, in order to restart the process, a new initial guess for the Newton method is required. Two strategies were employed to deal with this issue. The first strategy was to increase the stepsize of the continuation parameter and check if the process jumped over the gap. This involved some trial and error, but worked in instances where the gap was small enough. The second strategy was to stop close enough to a resonance, and then transition from the BCP to the

RBTP by decreasing the mass of the Sun. Once in the RTBP, the torus is a periodic orbit that can be easily continued until it crosses the resonance, and then go back to the BCP by increasing the mass of the Sun. Sometimes it is not necessary to reach the RTBP when decreasing the mass of the Sun, it is enough to lower its mass (this reduces the size of the gap) to continue the torus through the resonance and then to increase the mass to be again in the BCP.

The next section describes how these techniques were applied to find families of invariant tori in the BCP.

4 Dynamics around the L_2 point

The result of computing and continuing families of 2D invariant tori is showed in Figure 4. The horizontal axis represents the x component of the corresponding invariant curve of the Poincaré map when $\theta = 0$. The vertical axis is the rotation number. Several resonances have been identified in Figure 4 to illustrate the argument made in Section 3.3 about the gaps in the family. A total of six families were found. Two of these families are planar Lyapunov-type quasi-periodic orbits (families H1 and H2 in Figure 4), and four have a vertical component. Out of these four, two are Halo-like quasi-periodic orbits (for the moment being, we refer to them as Halo families of Type I and Type II, see Figure 4) and the other two fall behind the Moon (families V1 and V2 in Figure 4). The next paragraphs explain how these families were found and constructed, and provide details on the two Halo-like quasi-periodic families.

As explained in Section 3.3, the continuation process requires an initial torus. This initial torus usually is computed from a periodic orbit. In the context of the BCP two initial periodic orbits were used to find and continue families of invariant tori. The first periodic orbit is a Halo orbit in the RTBP. The approach is to pick one Halo orbit in RTBP, and then continue it with respect to the mass of the Sun until it reaches the BCP. This process had to be repeated multiple times with different Halo orbits due to the presence of gaps in the family of quasi-periodic Halo orbits. Figure 5 shows an example in different projections of how a Halo orbit in the RTBP becomes a quasi-periodic orbit in the BCP with two frequencies: the intrinsic one corresponding to the Halo orbit, and the one acquired due to the Sun's perturbation. The other periodic orbit used was the one found by continuing the L_2 point from the RTBP to the BCP. This orbit, described in Section 2, generates a family of planar quasi-periodic orbits. This family can be considered the quasi-periodic planar Lyapunov family counterpart of the periodic ones in the RTBP (family H1 in Figure 4). The stability of this family was analyzed, and most of the tori are hyperbolic. There is always an eigenvalue equal to 1 with multiplicity two, plus one real eigenvalue of the order of 10^6 (and its inverse), and another pair that evolves in a way that the family undergoes two bifurcations. This is illustrated in Figure 6, where the last pair of eigenvalues are plotted. The horizontal axis corresponds to the x component of the invariant curve, and the vertical axis the absolute value of the eigenvalue. Figure 6 shows that there are two bifurcations where the absolute value of the eigenvalues is equal to one. In these cases, there are two small intervals that contain partially elliptic tori; this is, that the eigenvalues are complex with norm equal to one. These small intervals are zoomed in Figure 7. The top row of Figure 7 shows the absolute value of the eigenvalues, and the bottom row the arguments. Note that a similar phenomena appears in the RTBP, where the planar Lyapunov family undergoes a bifurcation that gives rise to the well-know family of Halo orbits. The same

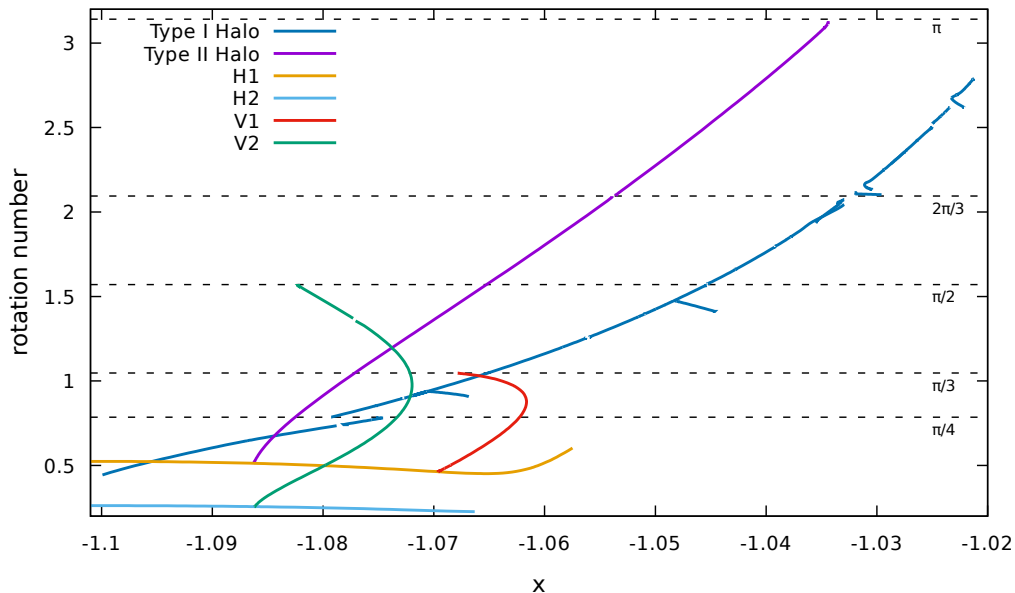


Figure 4: Families of invariant 2D tori in the BCP. See text for details.

happens in the BCP for these two bifurcations. Each one of this families can be continued along a vertical component.

During the continuation of the V1 family, it was found that some small resonances needed to be avoided. The strategy of going back to the RTBP by decreasing the mass of the Sun, continuing the resulting object there until the resonance is passed, and going back to the BCP was employed. After returning to the BCP, it was noticed that the resulting torus did not belong to the V1 family, but to a new one labeled as V2. This torus was continued, both increasing and decreasing the rotation number. Eventually, the V2 branch met a planar quasi-periodic Lyapunov orbit of a new family, called H2. Again, this family was continued, hence completing the picture represented in Figure 4. A complete study of the H and V families is left for another work, although some examples are provided in the Appendix. The next subsection elaborates on the Type I and Type II Halo-like families, the focus of this paper.

4.1 The Type I and Type II Halo-like families

Let us begin showing some representative examples of the members of these two families. The first example of Type I Halo family is shown in Figure 5. The rotation number of this torus is $\rho = 1.3800185497627542$. Another example is shown in Figure 8. In this case, the rotation number is $\rho = 2.6752268478193670$. This torus is close to the resonance value of $\rho = 6\pi/7 \approx 2.6927937\dots$. The effect of being close to a resonance is illustrated in Figure 9, a torus with rotation number $\rho = 2.6924643478193717$. Figure 10 shows a torus of the Type II family. This particular example has rotation number $\rho = 3.1161371680267869$. The projection on the $x - z$ plane shows that the orbit is a Halo-like in the sense that when observed from the Earth, the orbit circles around the L_2 point, leaving the Moon inside and hence allowing for a continuous line-of-sight between the Earth and the orbit.

Similarly to the case in the Type I Halo family, near a resonance we observe the same

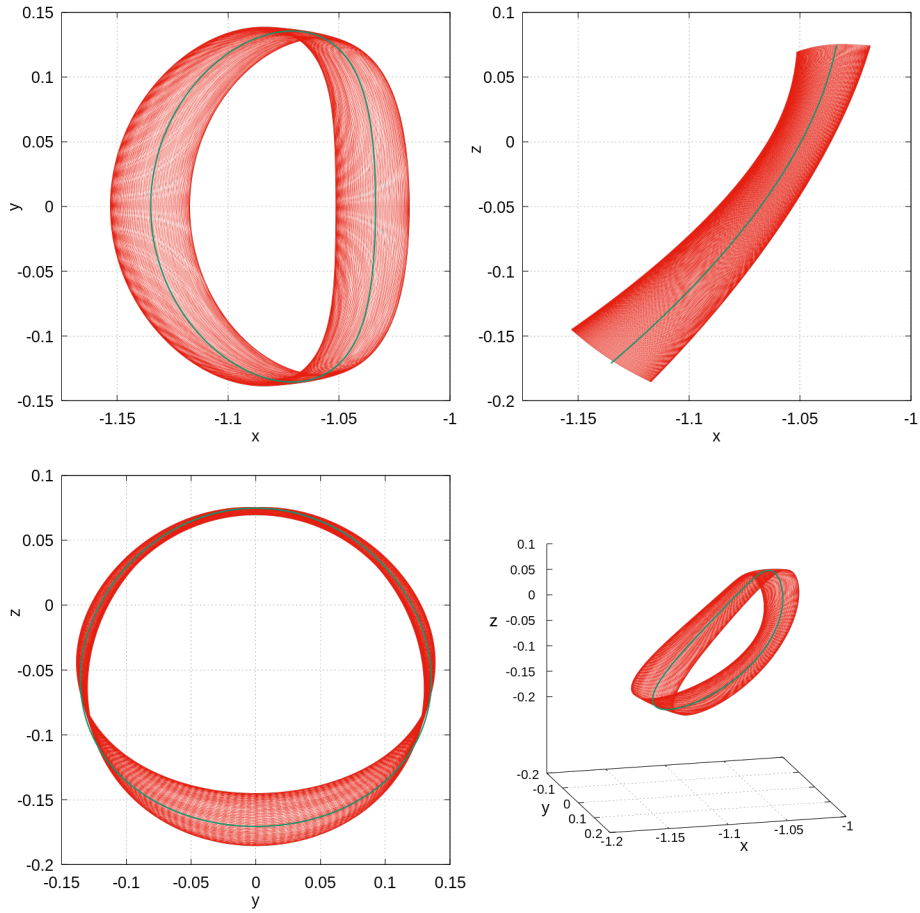


Figure 5: Transition from Halo orbit in the RTBP (green) to a torus in the BCP (red).

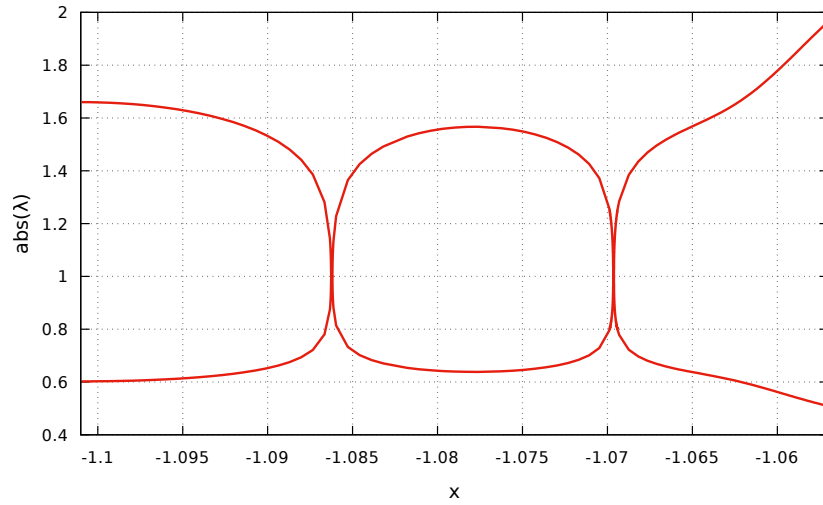


Figure 6: Stability of the planar quasi-periodic Lyapunov H1 family in the BCP

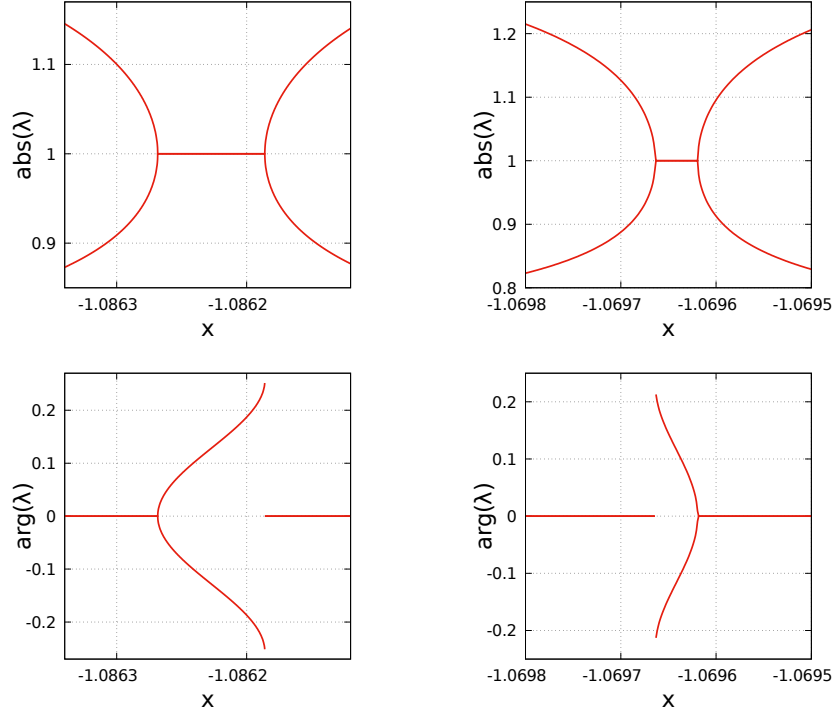


Figure 7: Zoom of the bifurcations in quasi-periodic Lyapunov family in the BCP

phenomena, and the orbit becomes more dense around the periodic orbit corresponding to that resonance. Figure 11 provides an example with rotation number equal to $\rho = 3.1303578715783535$, close the resonance $\rho = \pi$.

As it has been mentioned before, the Type I family of Halo-like orbits appears when adding the Sun effect to the family of Halo orbits of the RTBP: the (non-resonant) Halo orbits add the frequency of the Sun to its own frequency and become a quasi-periodic orbit with two basic frequencies. To better understand the Type II family, we continue them by decreasing the mass of the Sun down to zero, so they are orbits of the RTBP. As an example, in Figure 12, up, we have plotted two RTBP orbits that come from the continuation of the Type II orbits with rotation numbers $\rho = 0.7394766853097875$ and $\rho = 0.8587717051237963$. Then, we have performed the reduction to the center manifold around L_2 (Jorba [1999], Jorba and Masdemont [1999]). By means of the change of coordinates, we have sent initial data of each orbit to the center manifold coordinates. Then, we have plotted a Poincaré map for the level of energy of each orbit and we have marked the initial data of each orbit in the map with a big dot (with the same color used to plot the orbits). The results are shown in Figure 12, down. This shows that the Type II orbits come from quasi-halo orbits of the RTBP that have one of its two frequencies in resonance with the frequency of the Sun. In this way, the effect of the Sun does not add a new frequency and the quasi-halo is continued into the BCP as a quasiperiodic orbit with two basic frequencies that we refer as Type II.

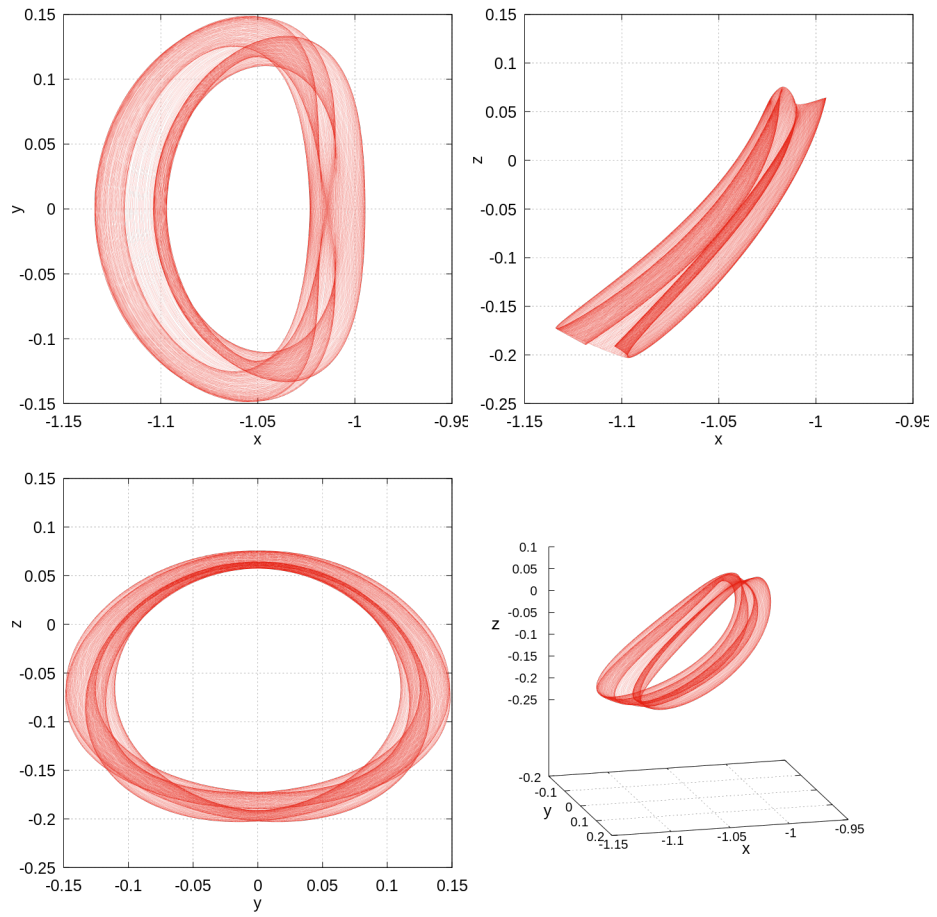


Figure 8: Different projections of a Type I Halo orbit.

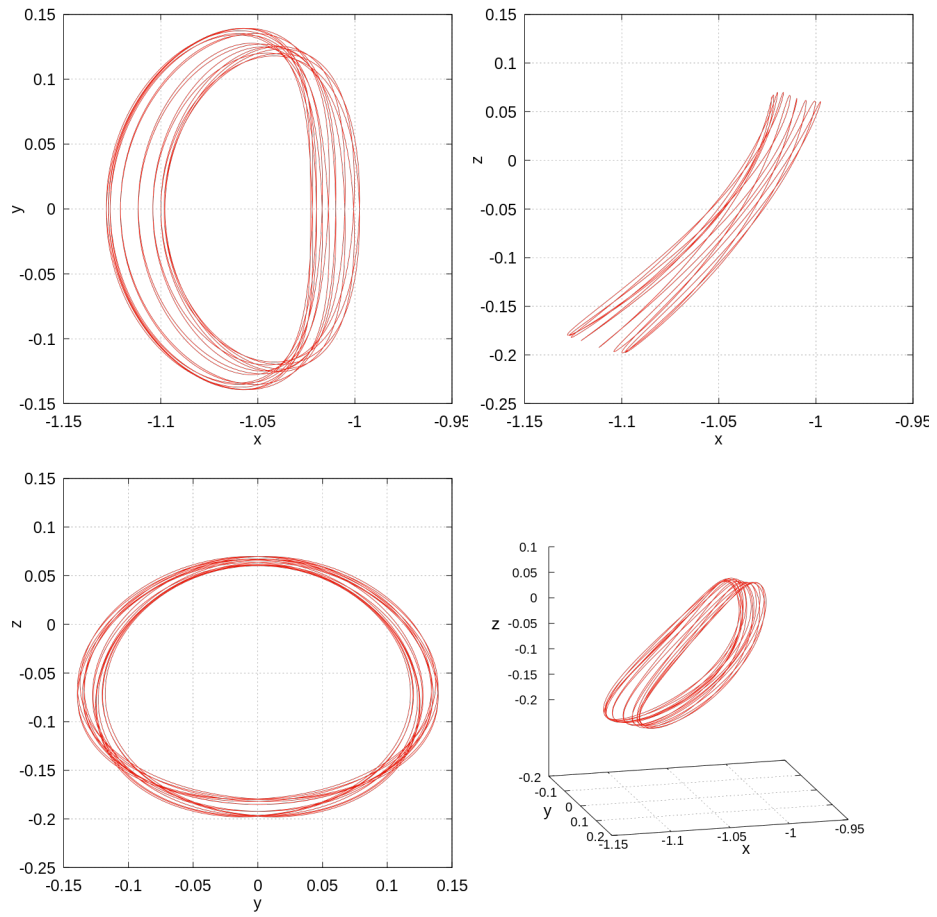


Figure 9: Different projections of a Type I Halo orbit near a resonance.

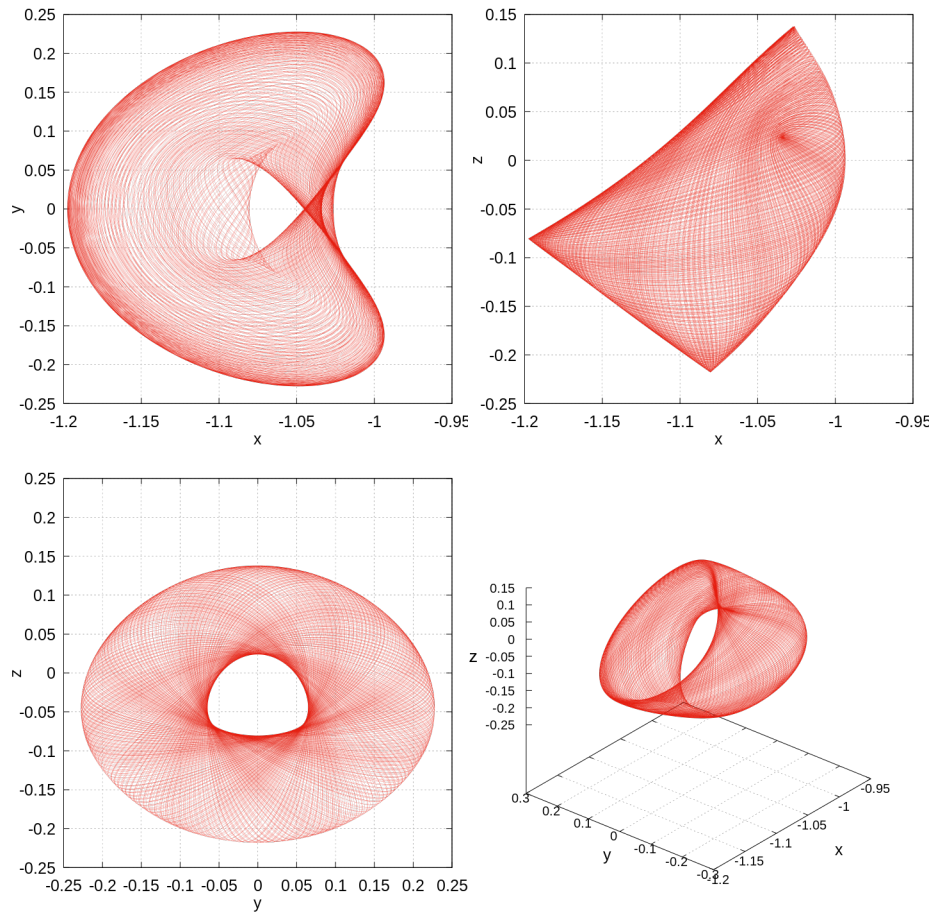


Figure 10: Different projections of a Type II Halo orbit.

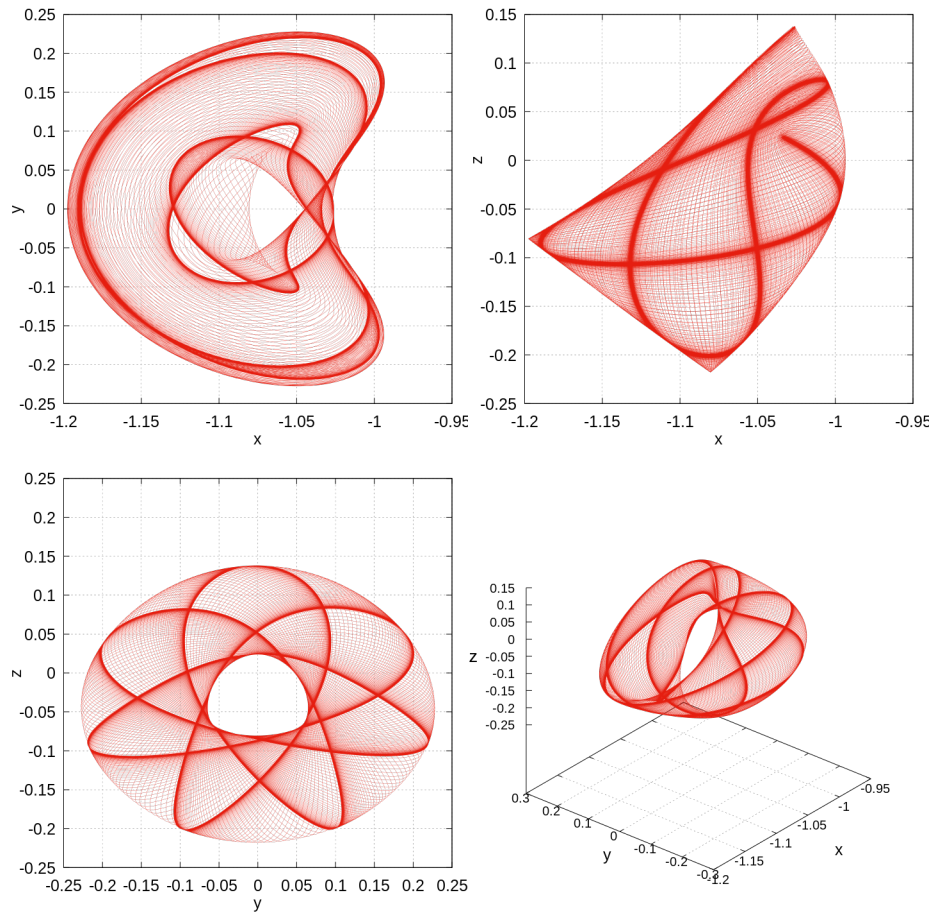


Figure 11: Different projections of a Type II Halo orbit near a resonance.

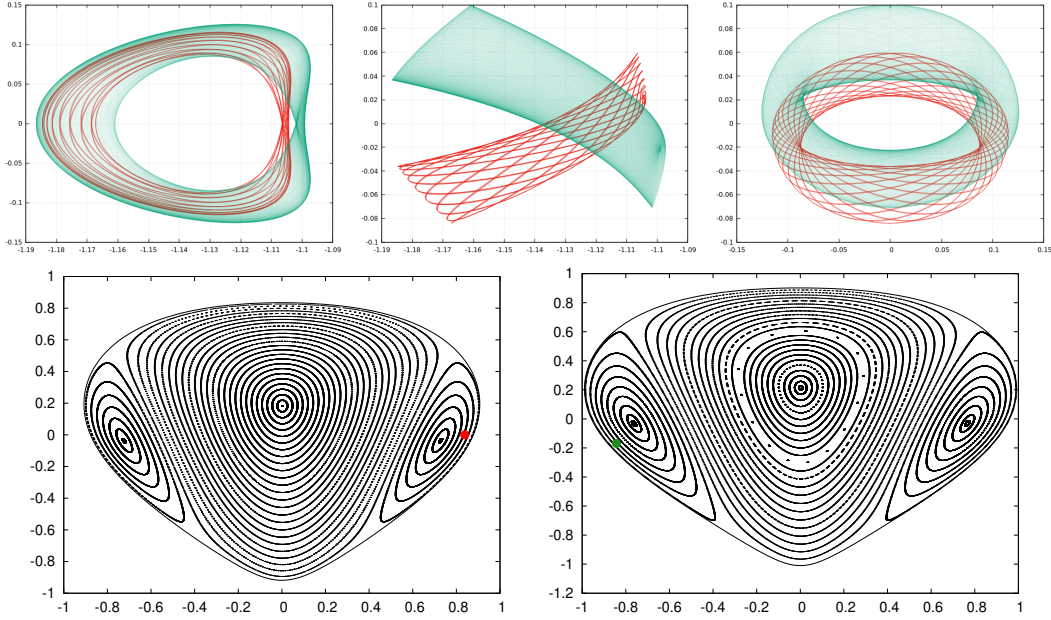


Figure 12: Up: (x, y) , (x, z) and (y, z) projections of two orbits of the RTBP that correspond to two orbits of the Type II Family. Down: These two orbits are marked (with the same color) in the Poincaré section of the center manifold of the RTBP at L_2 .

4.1.1 Stability

To fully characterize these orbits, we study their stability. Using the method described in Section 3.1, the stability of all the tori computed for each one of the families is obtained. For the Type I Halo family, they mostly behave like their counterparts in the RTBP, the Halo orbits. Due to the Hamiltonian structure, there is always the eigenvalue 1 with multiplicity two. For each tori of this family there is a large real eigenvalue (and its inverse), and, for almost each tori, a complex eigenvalue (and its inverse) with modulus 1. The absolute value of the latter pair of eigenvalues is shown in Figure 13 with respect to the x component of the invariant curve at $\theta = 0$. It is observed that most of these pairs of eigenvalues have modulus 1 with the exception of some isolated zones. However, the main takeaway is that most of the tori are partially elliptic with one saddle. On the other hand, the Type II Halo family has a different stability type. In this case, and as in the case of the Type I Halo family, there is always the eigenvalue 1 with multiplicity two. There is also a large real eigenvalue (and its inverse). The other pair, however, is also real and positive. Figure 14 shows the evolution of this eigenvalue with respect to the x component of the invariant curve at $\theta = 0$. Hence, the Type II Halo family has two saddles. We note that the largest eigenvalues of the Type I and Type II families are of the same order of magnitude.

4.2 Applications

The existence of two Halo-like families illustrates a resonance between the direct effect of the Sun's gravity, as modeled in the BCP, with a quasi-Halo orbit of the RTBP. We emphasize the dependency on how the effect of the Sun is accounted for because, for example, the QBCP also models the direct effect of the Sun's gravity but, as of today, only the quasi-periodic counterparts of the Halo orbits (Type I family) have been computed (see Andreu

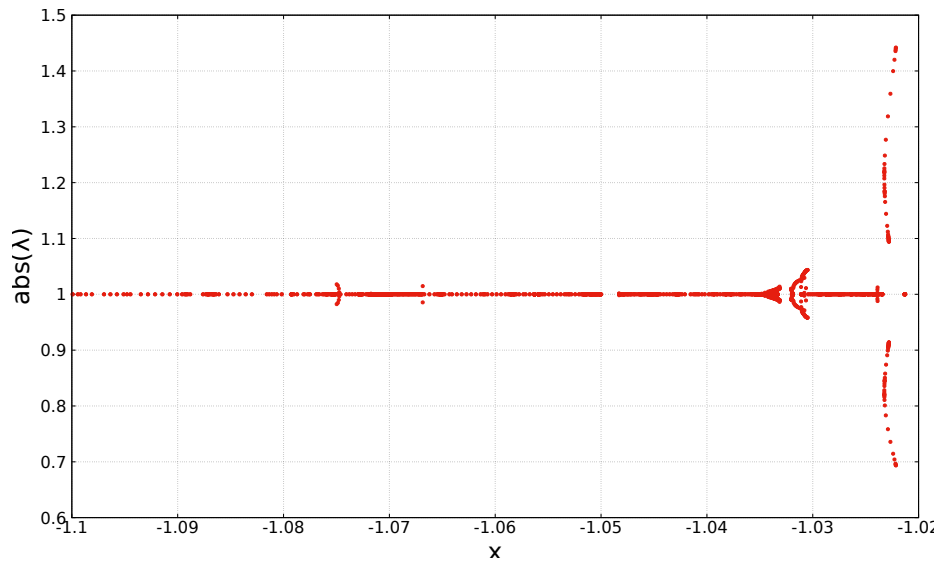


Figure 13: Absolute value of the second eigenvalue along the Type I Halo family in the BCP. See the text for more details.

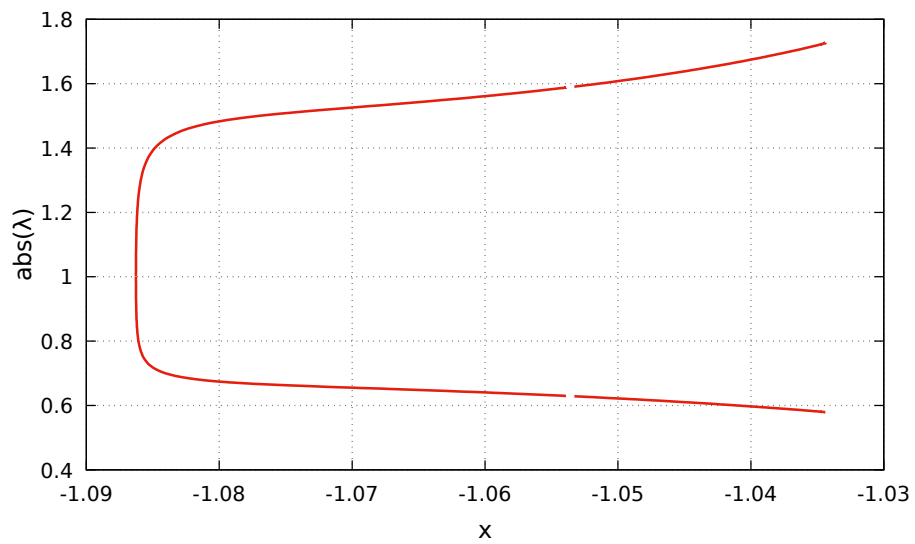


Figure 14: Absolute value of the second eigenvalue along the Type II Halo family in the BCP. See the text for more details.

[1998]). The existence of Type II Halo-like orbits in the QBPC is an open problem. Hence, the BCP has this feature that may be exploited for mission design: the existence of a second family with a similar topology to the Halo orbits, provides mission analysts with new potential candidates to meet the requirements for missions to the vicinity of the Moon.

However, when it comes to practical applications, there are some caveats that need to be addressed. The main one is that this work's objects of interest, the Type I and Type II families, need a counterpart in a real ephemeris model. The authors are aware that the usefulness of a model is limited by how well it captures the reality it tries to represent. There is numerical and experimental evidence that the Halo orbits in the Sun-Earth-Moon system exist in the real one. In Andreu [1998], using quasi-periodic Halo orbits in the QBPC and the DE403 JPL ephemeris, the author propagates for times intervals between 22 and 45 years Halo orbits of the Solar System. Hence, there is reason to believe that the same applies to the orbits in the BCP of the Type I family. However, for the Type II family there is no evidence that they are feasible in an ephemeris model. We may be in a situation where they do not survive the transition between the BCP and the ephemeris model. The study of the persistence of these families in a realistic model is work in progress.

Finally, let us comment a bit more on the Type II Halo family, that shares some topological features with Type I Halo family. This gives the mission designer more options to explore potential orbits for the mission. Note that there are representatives members of each family that are not blocked by the Moon, making them useful for missions to the neighborhood of the Moon that require constant contact to the Moon. Figure 15 shows the projection on the $x = 0$ plane corresponding to how these orbits would be seen from an observer in the Earth. The projections in Figure 15 correspond to the same orbits shown in Figures 10 and 11. In these figures, the center of the Moon is at the origin, and it has been plotted a circle with the approximated radius of the Moon, and another one with a circle twice the radius of the Moon. In both cases it is observed that there is continued line-of-sight between the Earth and the orbit. Finally, it is worth noting that in the particular case of the Type II Halo family, given that they are less stable, they would be most likely discarded to place a permanent station. However, their suitability for other applications would be always contingent to the mission requirements.

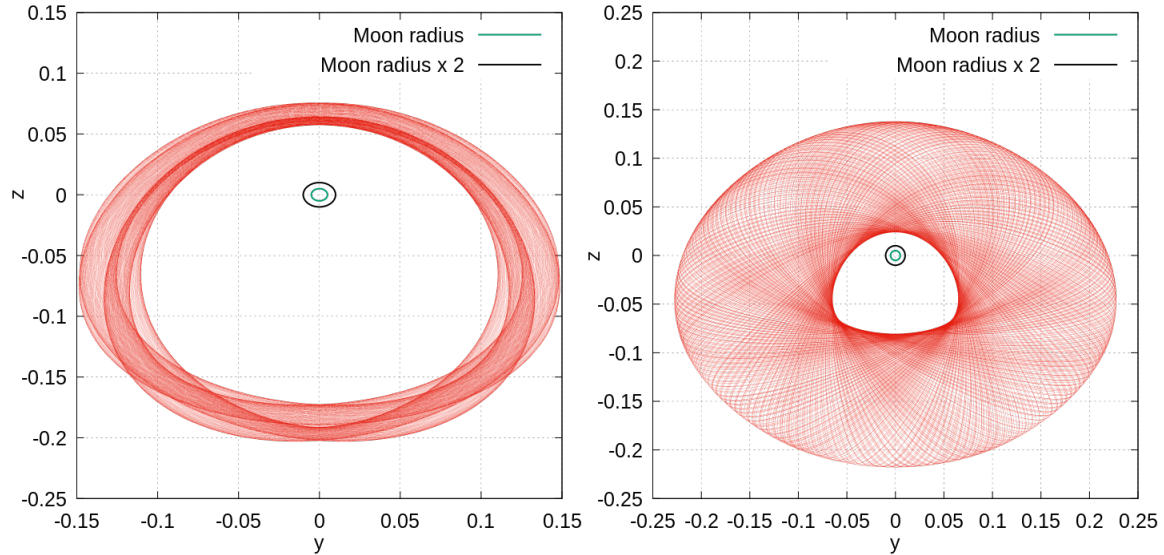


Figure 15: Type I (left) and Type II (right) Halo orbits as seen from the Earth with the Moon radius superimposed.

5 Conclusions and further work

In this paper we have explored the dynamics of a massless particle around L_2 in the Bicircular Problem. In this model, the L_2 point is only defined geometrically because it is not an equilibrium point. By means of a continuation scheme with respect to the Sun's effect, we showed that there is no natural dynamic replacement of the L_2 point in the BCP.

Continuation of invariant tori families was the technique adopted as an alternative to the reduction to the normal manifold, given that the size of the domain of validity of the expansions is too small to provide information about the dynamics in a reasonable neighborhood of the L_2 region. Following this approach, we have identified a total of six families. Out of these six families, two of them were planar quasi-periodic orbits, and the other four had vertical component. Out of these four three-dimensional families, two were Halo-like orbits. The first Halo-like family, called Type I Halo, were obtained by sampling and continuing their RTBP counterparts from the RTBP to the BCP. The second family, Type II Halo, was found by analyzing the bifurcation of the planar family H1.

The stability of the Halo-like orbits was computed. One family, the Type I Halo family, can be seen as the natural continuation of the classical Halo orbits of the RTBP and share the same stability type of their RTBP counterparts (saddle \times center \times center.. On the other hand, the Type II Halo family comes from a quasi-Halo orbit of the RTBP which has one frequency in resonance with the frequency of the Sun and their stability is of the type saddle \times saddle \times center. The topology of these two families makes them suitable to space missions, being the Type I Halo family probably more adequate given its stability type. There is, however, more work to be done. The future work is summarized in the following paragraph.

As first step, more work needs to be done to study the other families. We also believe that there are some more families of Halo-like quasi-periodic orbits with two basic frequencies, and more work is needed to find them. Although with no obvious application to space missions, they still have academic interest. In parallel, and focusing on mission analysis

and to the potential applications of the Halo-like families to mission design, we need study these families in a real ephemeris model and to develop station-keeping strategies. Second, how to transfer from the vicinity of the Earth to one of these orbits would also be of interest to the mission designer (Rosales et al. [2020]). To that effect, the use of the stable/unstable manifold would be very useful, as it has been proven very successfully in other contexts. This also would help to get a deeper understanding of the dynamical skeleton of the BCP around the L_2 point.

6 Appendix

In this section some examples of tori from the other families found are given (see Figure 4). They are provided here to illustrate the richness of the Sun-Earth-Moon BCP, and to evidence that the vertical families V1 and V2 are not Halo-like. A complete study of their stability properties and how they transition from the RTBP to the BCP is under work, and no details are provided here.

The planar tori from the families H1 and H2 are very similar, and two examples of each one are shown in Figure 16. The representative of the family H1 (left) has rotation number $\rho = 0.5226878126286740$. The rotation number of the representative of the family H2 (right) is $\rho = 0.2586841081044178$.

More interesting are the families V1 and V2 with a vertical component. Different projections of a representative of the family V1 with rotation number $\rho = 0.6510146280704701$ are shown in Figure 17. The projection onto the plane $x = 0$ (bottom-left image) shows that this orbit falls behind the Moon.

Finally, an example of the family V2 is illustrated in Figure 18. This torus has rotation number $\rho = 0.5852970529159898$. It also falls behind the Moon. However, the projection onto the plane $x = 0$ (bottom-left image) show that has different symmetry than the representative of the V1 family.

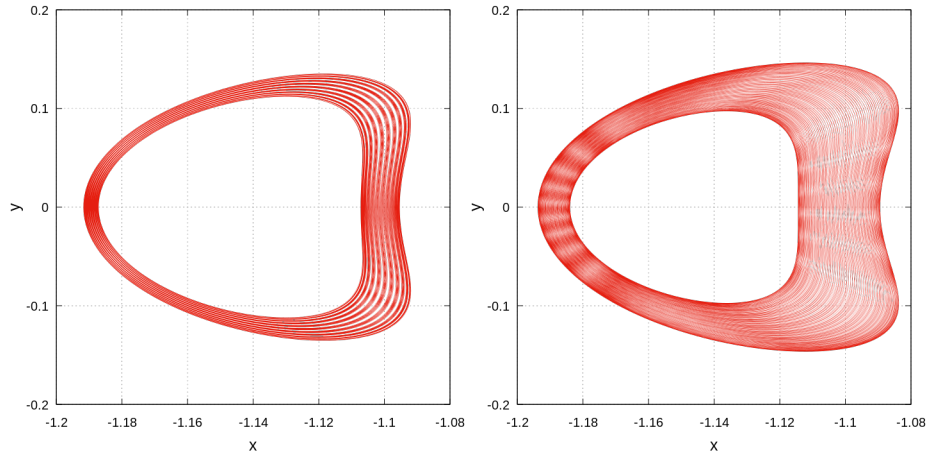


Figure 16: Projections of a H1 orbit (left) and a H2 orbit (right).

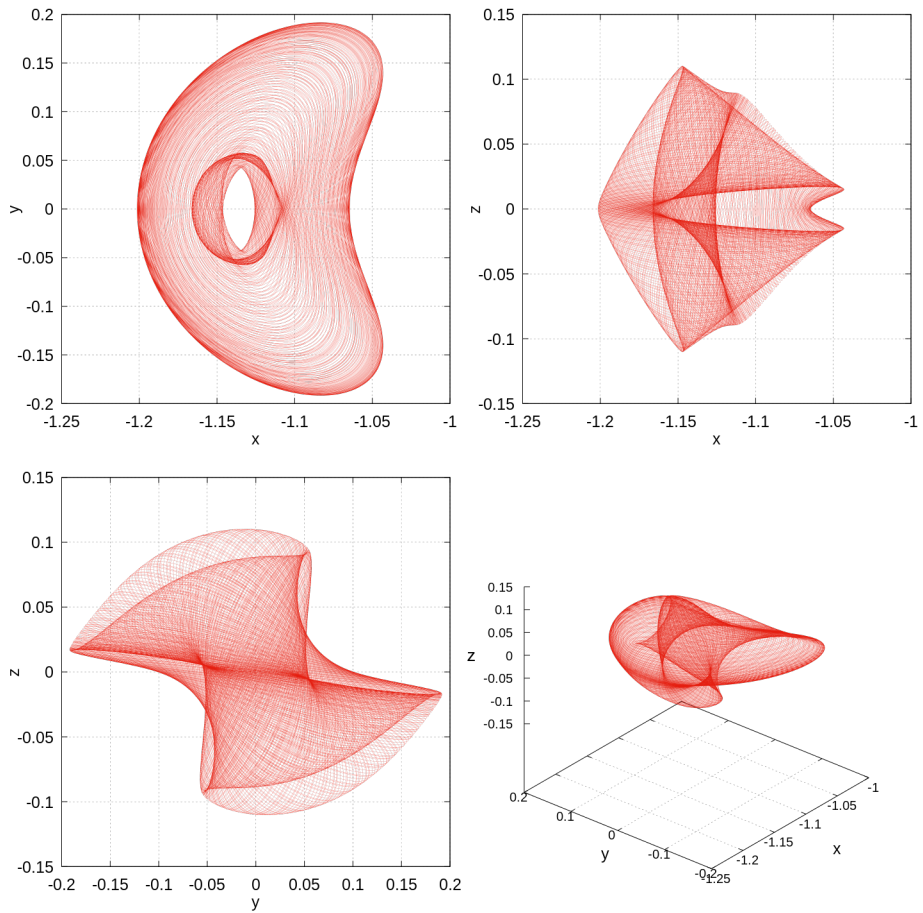


Figure 17: Different projections of a V1 orbit.

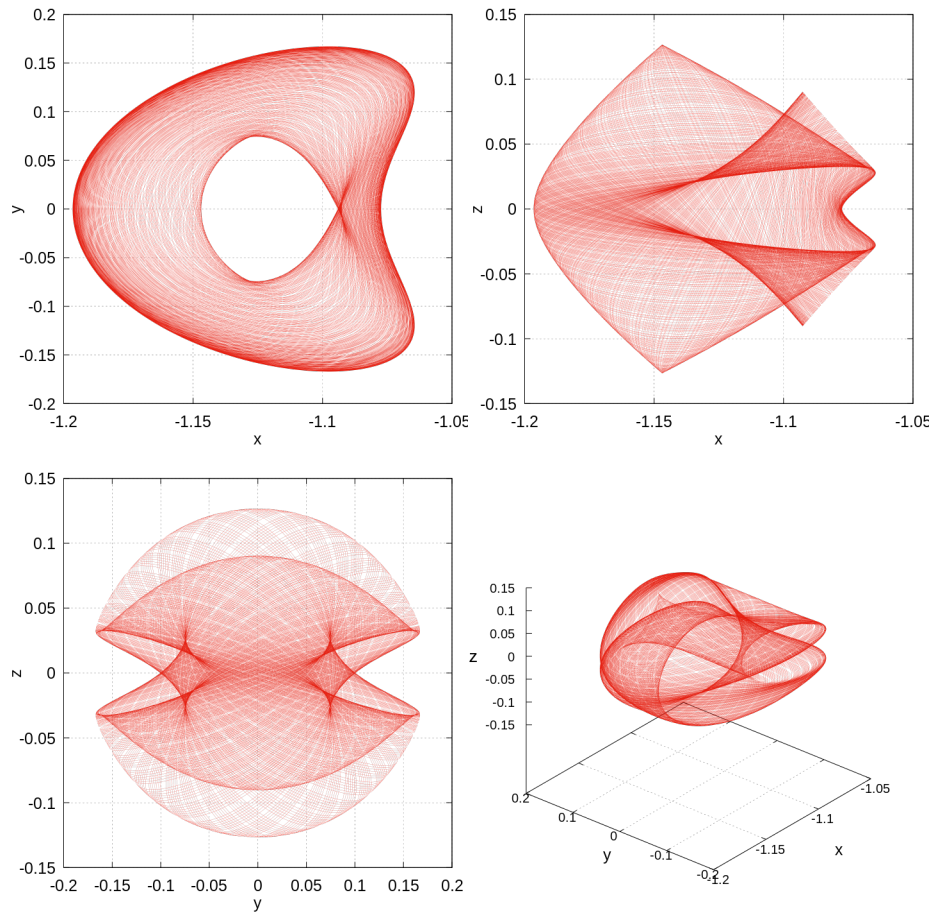


Figure 18: Different projections of a V2 orbit.

Conflict of interest

The authors declare that they have no conflict of interest.

References

- M. A. Andreu. *The Quasi-Bicircular Problem*. PhD thesis, Univ. Barcelona, 1998.
- M. A. Andreu. Dynamics in the center manifold around L_2 in the Quasi-Bicircular Problem. *Celestial Mech.*, 84(2):105–133, Oct 2002. ISSN 1572-9478. doi: 10.1023/A:1019979414586. URL <https://doi.org/10.1023/A:1019979414586>.
- J. Breakwell and J. Brown. The ‘Halo’ family of 3-dimensional periodic orbits in the Earth-Moon restricted 3-body problem. *Celestial Mech.*, 20(4):389–404, 1979.
- J. Carr. *Applications of centre manifold theory*. Applied mathematical sciences. Springer-Verlag, New York, 1981. URL <http://opac.inria.fr/record=b1090651>. Based on a series of lectures given in the Lefschetz Center for Dynamical Systems in the Division of Applied Mathematics at Brown University during the academic year 1978-79–Pref.
- E. Castellà. *Sobre la dinàmica prop dels punts de Lagrange del sistema Terra-Lluna*. PhD thesis, Universitat de Barcelona, 2003.
- E. Castellà and À. Jorba. On the vertical families of two-dimensional tori near the triangular points of the bicircular problem. *Celestial Mech.*, 76(1):35–54, Jan 2000. ISSN 1572-9478. doi: 10.1023/A:1008321605028. URL <https://doi.org/10.1023/A:1008321605028>.
- J. Cronin, P. Richards, and L. Russell. Some periodic solutions of a four-body problem. *Icarus*, 3:423–428, 1964.
- G. Duarte. *On the dynamics around the collinear points in the Sun-Jupiter system*. PhD thesis, Universitat de Barcelona, 2020.
- A. Farrés and À. Jorba. On the high order approximation of the centre manifold for odes. *Discrete and Continuous Dynamical Systems - Series B*, 14(3):977–1000, 2010. ISSN 1531-3492. doi: 10.3934/dcdsb.2010.14.977. URL <http://aimsciences.org/journals/displayArticlesnew.jsp?paperID=5350>.
- G. Gómez and J. Mondelo. The dynamics around the collinear equilibrium points of the RTBP. *Physica D: Nonlinear Phenomena*, 157(4):283 – 321, 2001. ISSN 0167-2789. doi: [https://doi.org/10.1016/S0167-2789\(01\)00312-8](https://doi.org/10.1016/S0167-2789(01)00312-8). URL <http://www.sciencedirect.com/science/article/pii/S0167278901003128>.
- G. Gómez, À. Jorba, J. Masdemont, and C. Simó. *Dynamics and Mission Design Near Libration Points: Volume IV: Advanced Methods for Triangular Libration Points*, volume 5. World Scientific, 2001a.
- G. Gómez, J. Llibre, R. Martínez, and C. Simó. *Dynamics and mission design near libration points. Vol. II, Fundamentals: the case of triangular libration points*, volume 3 of *World Scientific Monograph Series in Mathematics*. World Scientific Publishing Co. Inc., 2001b. ISBN 981-02-4274-3.

- J. Gonzalez and J. Mireles James. High-order parameterization of stable/unstable manifolds for long periodic orbits of maps. *SIAM Journal on Applied Dynamical Systems*, 16, 09 2016. doi: 10.1137/16M1090041.
- S. Huang. Very restricted four-body problem. Technical note TN D-501, Goddard Space Flight Center, NASA, 1960. URL <https://ntrs.nasa.gov/archive/nasa/casi.ntrs.nasa.gov/19890068606.pdf>.
- À. Jorba. A methodology for the numerical computation of normal forms, centre manifolds and first integrals of Hamiltonian systems. *Exp. Math.*, 8(2):155–195, 1999.
- À. Jorba. Numerical computation of the normal behaviour of invariant curves of n -dimensional maps. *Nonlinearity*, 14(5):943–976, jul 2001. doi: 10.1088/0951-7715/14/5/303. URL <https://doi.org/10.1088/0951-7715/14/5/303>.
- À. Jorba and J. Masdemont. Dynamics in the center manifold of the collinear points of the restricted three body problem. *Physica D Nonlinear Phenomena*, 132:189–213, July 1999. doi: 10.1016/S0167-2789(99)00042-1.
- À. Jorba and B. Nicolás. Transport and invariant manifolds near L_3 in the Earth-Moon Bicircular model. Preprint, 2020.
- À. Jorba and E. Olmedo. On the computation of reducible invariant tori on a parallel computer. *SIAM J. Appl. Dyn. Syst.*, 8(4):1382–1404, 2009.
- À. Jorba and J. Villanueva. On the persistence of lower dimensional invariant tori under quasi-periodic perturbations. *Journal of Nonlinear Science*, 7(5):427–473, Oct 1997. ISSN 1432-1467. doi: 10.1007/s003329900036. URL <https://doi.org/10.1007/s003329900036>.
- À. Jorba, M. Jorba-Cuscó, and J. J. Rosales. The vicinity of the Earth-Moon L_1 point in the Bicircular Problem. *Celestial Mech.*, 132(2):11, Feb 2020. doi: 10.1007/s10569-019-9940-2. URL <https://doi.org/10.1007/s10569-019-9940-2>.
- M. Jorba-Cuscó, A. Farrés, and À. Jorba. Two periodic models for the Earth-Moon system. *Frontiers in Applied Mathematics and Statistics*, 4:32, 2018. ISSN 2297-4687. doi: 10.3389/fams.2018.00032. URL <https://www.frontiersin.org/article/10.3389/fams.2018.00032>.
- B. Le Bihan, J. Masdemont, G. Gómez, and S. Lizy-Destrez. Invariant manifolds of a non-autonomous quasi-bicircular problem computed via the parameterization method. *Nonlinearity*, 30:3040–3075, 2017.
- J. Rosales, À. Jorba, and M. Jorba-Cuscó. The effect of the Sun on direct transfers from Earth to translunar Halo orbits. In preparation, 2020.
- D. J. Scheeres. The restricted Hill four-body problem with applications to the Earth-Moon-sun system. *Celestial Mech.*, 70(2):75–98, Feb 1998. ISSN 1572-9478. doi: 10.1023/A:1026498608950. URL <https://doi.org/10.1023/A:1026498608950>.
- R. Seydel. *Practical bifurcation and stability analysis*. Interdisciplinary Applied Mathematics (Vol 5). Springer-Verlag, New York, third edition, 2009. URL <https://doi.org/10.1007/978-1-4419-1740-9>.

- J. Sijbrand. Properties of center manifolds. *Trans. Amer. Math. Soc.*, 289(2):431–469, 1985. ISSN 0002-9947.
- C. Simó, G. Gómez, À. Jorba, and J. Masdemont. The Bicircular model near the triangular libration points of the RTBP. In A. Roy and B. Steves, editors, *From Newton to Chaos*, pages 343–370, New York, 1995. Plenum Press.
- J. Stoer and R. Bulirsch. *Introduction to numerical analysis*, volume 12 of *Texts in Applied Mathematics*. Springer-Verlag, New York, third edition, 2002. ISBN 0-387-95452-X. doi: 10.1007/978-0-387-21738-3. URL <http://dx.doi.org/10.1007/978-0-387-21738-3>.
- A. Vanderbauwhede. Centre manifolds, normal forms and elementary bifurcations. In *Dynamics reported, Vol. 2*, volume 2 of *Dynam. Report. Ser. Dynam. Systems Appl.*, pages 89–169. Wiley, Chichester, 1989.